Excitation functions of the α-particle-induced reactions on ^{nat}Cr up to 50 MeV

N. Ukon[a,*,†], M. Aikawa[a], Y. Komori[b], H. Haba[b], F. Ditrói[c], S. Takács[c]

[a] Faculty of Science, Hokkaido University, Sapporo 060-0810, Japan

[b] Nishina Center for Accelerator-Based Science, RIKEN, Wako 351-0198, Japan

[c] Institute for Nuclear Research (ATOMKI), 4026 Debrecen, Hungary

Keyword

Iron-52; Alpha particle irradiation; Chromium target; Excitation function; Cross section

Abstract

Activation cross sections of the α-particle-induced reactions on ^{nat}Cr were measured. A stacked foil activation technique and γ-ray spectrometry were used. Nickel-chromium alloy, nickel and titanium metallic foils were stacked as a target. The target was irradiated with a 51.2-MeV α-particle beam at the AVF cyclotron, RIKEN. The γ rays were measured for the irradiated foils using an HPGe detector. Production cross sections of ^{52g}Fe, ^{52g,54}Mn, ^{48,51}Cr and ^{48}V radionuclides were determined. The cross sections determined in this experiment were compared with the literature data and found to be consistent with them.

1. Introduction

The radionuclide ^{52g}Fe has a half-life of 8.275 h and decays with EC and β^+ decay modes by emitting an intense γ ray at 849.43 keV (I_γ =100%) [1]. The β^+ particle generates annihilation γ rays at 511.0 keV. These γ lines can be used for medical diagnostic imaging such as single photon emission computed tomography (SPECT) and positron emission tomography (PET) in particular for PET bone marrow imaging [2-6]. ^{52g}Fe decays to ^{52m}Mn ($T_{1/2}$ = 21.1 min), which mostly decays with emission of a positron (98.25%) and is a potential medical radioisotope for PET [7]. ^{52g}Fe is thus a valuable radionuclide and investigations of its production routes are necessary for optimizing its production.

There are several possible reactions to produce ^{52g}Fe. The Coordinated Research Project of International Atomic Energy Agency showed evaluation of available experimental results and recommended cross sections for possible production reactions [8], such as the ^{55}Mn(p,4n)^{52}Fe [9], ^{nat}Ni(p,x)^{52}Fe and ^{50}Cr(α,2n)^{52}Fe reactions [10]. In this paper we focus on the ^{50}Cr(α,2n)^{52}Fe reaction. There are only three experiments [11-13] in the EXFOR library [14] and additional one [15] in a literature survey. One of the experimental data [12] shows a large deviation from the others. Therefore,

* Corresponding author: ukon@fmu.ac.jp

† Present address: Advanced Clinical Research Center, Fukushima Medical University, Fukushima City 960-1295, Japan

we performed an experiment to measure the cross sections of the $^{nat}Cr(\alpha,x)^{52}Fe$ reaction. Since below the threshold energy of the $^{52}Cr(\alpha,4n)^{52}Fe$ reaction (39.8 MeV), only the $^{50}Cr(\alpha,2n)^{52g}Fe$ reaction contributes to the cross sections of the $^{nat}Cr(\alpha,x)^{52}Fe$ process. Thus, the cross sections measured on natural chromium can be normalized to those of ^{50}Cr.

In addition to the $^{50}Cr(\alpha,2n)^{52}Fe$ reaction, we determined activation cross sections for the reactions to produce $^{52g,54}Mn$, $^{48,51}Cr$ and ^{48}V in this work.

2. Experimental

An experiment to measure the activation cross sections of the α-particle-induced reactions on ^{nat}Cr was performed at the AVF cyclotron of RIKEN. The standard stacked foil activation technique and high resolution γ-ray spectrometry were used to determine the cross sections.

Nickel-chromium alloys (NiCr) were used because chromium is difficult to process into a foil structure. Nickel foil was stacked in order to compare it with nuclides produced from nickel in NiCr, and titanium was used for the monitored reactions. All the foils were purchased from Nilaco Corp., Japan. The NiCr foils were used as targets of ^{nat}Cr, which has four stable isotopes as listed in Table 1 [16]. Composition and the thicknesses of the used foils are shown in Table 2. The elemental analysis of the NiCr was conducted by scanning electron microscopy with energy dispersive spectroscopy using JSM-6610LA with JED-2300, JEOL Ltd. at Hokkaido Research Organization. The measured weight percentage of ^{nat}Cr in the alloy is 20.1 ± 0.1%, which is consistent with the nominal value of 20 ± 1%. The surface areas and weights of the large foils were first measured to determine the average thicknesses. Then the foils were cut into 10×10 mm^2 to fit into the target holder. The target holder served also as a Faraday cup. No electron suppression voltage was applied for the Faraday cup, since the solid angle for the possible escaping secondary electrons was negligibly small. The stacked target consisted of 10 sets of 2 or 3 NiCr, 2 Ni and 2 Ti foils (NiCr-NiCr-NiCr-Ni-Ni-Ti-Ti foils for 4th-7th sets and NiCr-NiCr-Ni-Ni-Ti-Ti foils for the others). The second and third foils in the same element foils were used for cross section deductions taking into account recoil compensation. The $^{nat}Ti(\alpha,x)^{51}Cr$ monitor reaction was used to check the beam parameters (energy and intensity) and validate the energy scale deduced from the calculated energy loss of the α particles throughout the layered target.

Table 1. Isotopic composition of natural chromium.

^{50}Cr	4.345%
^{52}Cr	83.789%
^{53}Cr	9.501%
^{54}Cr	2.365%

Table 2. Composition and thicknesses of the foils.

	Nickel-chromium	Ni	Ti
Composition	Cr 20.1(1)% Ni 79.9(2)%	Ni >99%	Ti 99.6%
Thickness (mg/cm^2)	6.17	4.15	2.43

The stacked target was irradiated with a 51.2 ± 0.2-MeV α-particle beam. The incident energy of the α particles was measured by the time-of-flight method [17]. Energy degradation in the target was calculated by using the SRIM code [18]. The irradiation with an average beam intensity of 209.8 nA lasted for 2 hours. The beam intensity was recorded every minute to check the beam stability during the irradiation.

The γ-ray spectra of the irradiated foils were measured by an HPGe detector (ORTEC GEM-25185-P) and analyzed by a dedicated software (SEIKO EG&G Gamma Studio). The detector was calibrated by a standard γ-ray point source containing mixture of the ^{57,60}Co, ^{88}Y, ^{109}Cd, ^{113}Sn, ^{137}Cs, ^{139}Ce and ^{241}Am radioisotopes. The reaction and decay data used in the data analysis were taken from online databases, NuDat 3.0[19], LiveChart [20, 21], QCalc [22] and the Nuclear Data Sheets [1, 23-25] and are summarized in Table 3.

Table 3. Reaction and decay data used in data analysis were taken from online databases [1, 19-25].

Nuclide	Half-life	Decay mode (%)	E_γ (keV)	I_γ (%)	Contributing reaction	Q-value (MeV)
^{52g}Fe	8.275 h	EC+β^+ (100)	849.43	100	^{50}Cr(α,2n)	-15.6
					^{52}Cr(α,4n)	-36.9
					^{53}Cr(α,5n)	-44.9
^{52g}Mn	5.591 d	EC+β^+ (100)	744.233	90.0(12)	^{50}Cr(α,d)	-10.3
					^{52}Cr(α,tn)	-25.3
					^{53}Cr(α,t2n)	-33.2
					^{54}Cr(α,t3n)	-43.0
					^{52}Fe decay	
^{54}Mn	312.20 d	EC+β^+ (100)	834.848	99.9760(10)	^{52}Cr(α,d)	-10.6
					^{53}Cr(α,t)	-12.3
					^{54}Cr(α,tn)	-22.0
^{51}Cr	27.7025 d	EC+β^+ (100)	320.0824	9.910(10)	^{50}Cr(α,3He)	-11.3
					^{52}Cr(α,αn)	-12.0
					^{53}Cr(α,α2n)	-20.0
					^{54}Cr(α,α3n)	-29.7

					^{51}Fe decay	
					^{51}Mn decay	
^{48}Cr	21.56 h	EC+β^+ (100)	112.31	96.0(20)	^{50}Cr(α,α2n)	-23.6
					^{52}Cr(α,α4n)	-44.9
^{48}V	15.9735 d	EC+β^+ (100)	983.525	99.98(4)	^{50}Cr(α,αd)	-18.9
					^{52}Cr(α,αtn)	-34.0
					^{53}Cr(α,αt2n)	-41.9
					^{48}Cr decay	

Reaction with the smallest Q-value is listed for every target isotope.

3. Results

The cross sections of the ^{nat}Ti(α,x)^{51}Cr monitor reaction were derived to assess the beam parameters and to check the foil thicknesses. The activity of ^{51}Cr in each Ti foil was determined by measuring the γ line at 320.0824 keV (I_γ = 9.910%) from the decay of ^{51}Cr ($T_{1/2}$ = 27.7025 d) after a cooling time of 90 days. The cross sections deduced using the measured experimental parameters were compared with the IAEA recommended values [26]. Based on the comparison, the incident beam energy was corrected by +0.2 MeV. The corrected cross-section data and the IAEA recommended values [26] are shown in Fig. 1. The experimental cross-section data are in good agreement with the recommended values. Based on the monitor reaction no additional correction was applied for the initial intensity and target thicknesses.

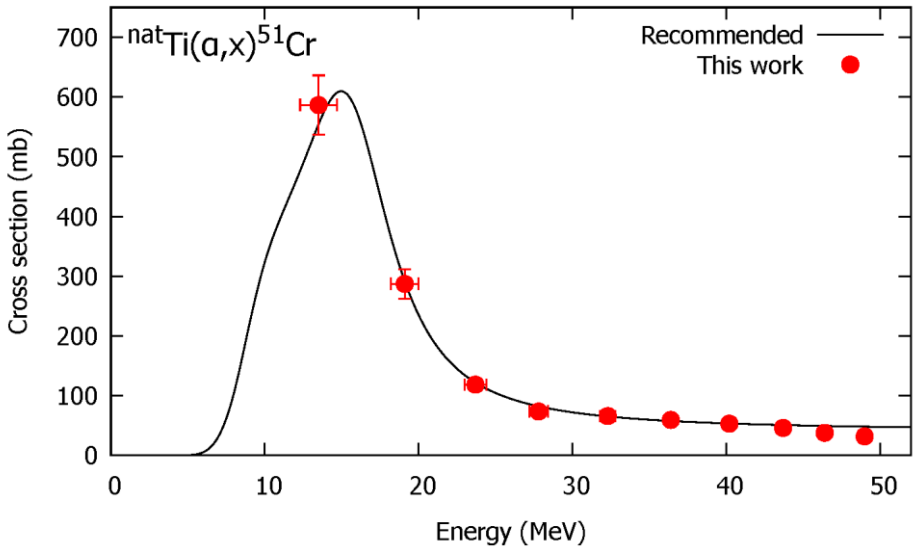

Fig. 1. Excitation function of the ^{nat}Ti(α,x)^{51}Cr monitor reaction with the recommended values [26].

The cross sections of the $^{nat}Cr(\alpha,x)^{52g}Fe$, $^{nat}Cr(\alpha,x)^{52g,54}Mn$, $^{nat}Cr(\alpha,x)^{48,51}Cr$ and $^{nat}Cr(\alpha,x)^{48}V$ reactions were derived in this experiment. The results are presented numerically in Table 4 and graphically in Figs. 2-7. The results are compared with the available experimental data measured earlier [11-13,15] as well as with the results of the TALYS model code taken from the TENDL-2021 data library [27].

The estimated total uncertainty of the cross sections was 10.0-30.7% except for one data point (53.3%) of the $^{nat}Cr(\alpha,x)^{51}Cr$ reaction close to its threshold energy. The uncertainties were estimated from the square root of the quadratic summation of each component; statistical uncertainty (0.4-29.0% with one exception of 52.4%), target thickness (measurement of lateral size and weight: 2%), target purity (nominal value: 5%), beam intensity (fluctuation in time and secondary electron emission: 5%), detector efficiency (activity of the standard source and polynomial fitting: 5%), γ intensity (derived values from online databases: <2.1%), and peak fitting (dependence on the fitting method, Covel method or Gaussian fitting: 3%).

Table 4. Activation cross sections determined on natural chromium target

Energy (MeV)	^{52g}Fe (mb)	^{54}Mn (mb)	$^{52g}Mn^{(cum)}$ (mb)	$^{51}Cr^{(cum)}$ (mb)	^{48}Cr (mb)	^{48}V (mb)
50.5 ±0.2	0.37 ±0.05	120 ±12	74 ±7	118 ±12	0.39 ±0.04	9.1 ±1.0
48.0 ±0.2	0.26 ±0.06	143 ±15	44 ±4	131 ±13	0.32 ±0.05	8.5 ±0.9
45.3 ±0.2	0.16 ±0.05	163 ±17	21 ±2	153 ±15	0.19 ±0.03	7.2 ±0.8
42.6 ±0.3	0.21 ±0.06	202 ±20	10 ±1	175 ±18	0.093 ±0.025	5.2 ±0.6
41.9 ±0.3	0.24 ±0.06	265 ±27	8.9 ±0.9	200 ±20		2.8 ±0.3
39.0 ±0.3	0.43 ±0.08	267 ±27	9.2 ±0.9	205 ±21		1.9 ±0.2
38.2 ±0.3	0.47 ±0.08	358 ±36	13 ±1	209 ±21		
35.1 ±0.4	0.50 ±0.08	387 ±39	14 ±1	208 ±21		
34.3 ±0.4	0.78 ±0.10	462 ±46	19 ±2	170 ±17		
30.9 ±0.5	0.73 ±0.10	478 ±48	20 ±2	161 ±16		
30.0 ±0.5	0.69 ±0.08	479 ±48	22 ±2	103 ±10		
26.2 ±0.6	0.57 ±0.07	477 ±48	22 ±2	83 ±8		
21.9 ±0.8	0.44 ±0.08	387 ±39	19 ±2	13 ±2		
16.9 ±1.0		54 ±5	3.6 ±0.4	0.13 ±0.07		

3.1 The $^{nat}Cr(\alpha,x)^{52g}Fe$ reaction

The radionuclide ^{52}Fe has a metastable state with a short half-life ($T_{1/2}$ = 45.9 s). The ^{52m}Fe metastable state decays almost 100% to ^{52g}Mn (EC+β^+: 100%) and in minor part to ^{52g}Fe (IT: <4.0E-3%). The latter contribution to populate the ^{52g}Fe state is negligibly small and the independent cross sections of the $^{nat}Cr(\alpha,x)^{52g}Fe$ reaction could be obtained by measuring the 168.688-keV γ line (I_γ = 99%) from the decay of ^{52g}Fe ($T_{1/2}$ = 8.275 h). The measurement series was started after a cooling time of 23 hours to reduce background. Our result is compared with the experimental data [11-13,15], the recommended values [8] and the TENDL-2021 data [27] in Fig. 2. The literature data presented for the $^{50}Cr(\alpha,x)^{52g}Fe$ reaction were normalized to the ^{nat}Cr target composition by taking into account the isotope ratio listed in Table 1. The experimental dataset reported by Chowdhury et al. (1995) was much larger than the other experimental datasets. Our result is consistent with the previous studies by Levkovski (1991) and Hermanne et al. (2015) and the recommended values [8] up to 45 MeV even above the threshold energy of 39.8 MeV for the $^{52}Cr(\alpha,4n)^{52g}Fe$ reaction. Above 45 MeV, the $^{52}Cr(\alpha,4n)$ reaction starts to contribute to the production of ^{52g}Fe. The TENDL-2021 data are different from the experimental ones in both amplitude and energy scale.

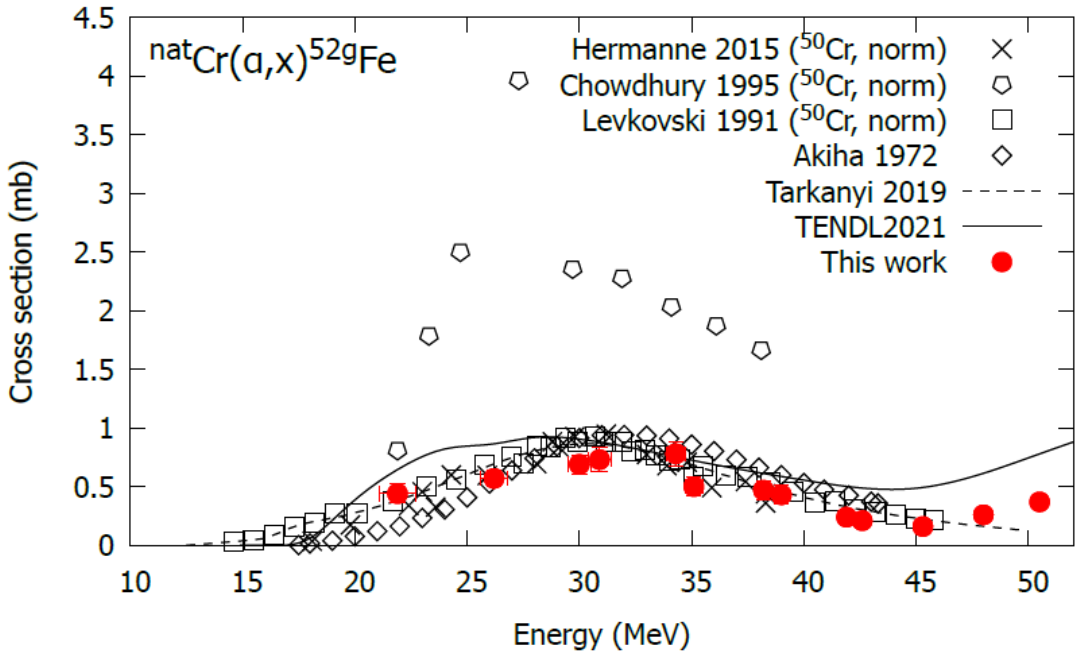

Fig. 2. Cross sections of the $^{nat}Cr(\alpha,x)^{52g}Fe$ reaction in comparison with the previous data [11-13, 15], the recommended values [8] and the TENDL-2021 result [27]. The values, normalized for the abundance of ^{nat}Cr are shown in the figure.

3.2 The $^{nat}Cr(\alpha,x)^{52g}Mn$ reaction

The radionuclide ^{52}Mn has a metastable state with a short half-life ($T_{1/2}$ = 21.1 min), which in most part decays to ^{52}Cr (EC+β^+: 98.25%) and in minor part to ^{52g}Mn (IT: 1.75%). Its ground state ^{52g}Mn ($T_{1/2}$ = 5.591 d) can be produced directly and also from the decays of ^{52m}Mn and $^{52g, 52m}Fe$. The γ line at 744.233 keV (I_γ = 90.0%) from the decay of ^{52g}Mn was used to assess the activity after a cooling time of 69 hours. Cumulative cross sections of the $^{nat}Cr(\alpha,x)^{52g}Mn$ reaction were determined including the direct and decay production. The results are compared with the previous studies [11-13] and the TENDL-2021 data [27] in Fig. 3. The cross sections measured on ^{50}Cr in the previous studies were normalized to those on ^{nat}Cr although the $^{52}Cr(\alpha,tn)^{52}Mn$ reaction contributes to the production of ^{52}Mn above the threshold energy of 27.3 MeV. Our results are in good agreement with the earlier experimental data by Levkovski (1991) and Hermanne et al. (2015) up to 40 MeV. The agreement would indicate that the contribution of the $^{52}Cr(\alpha,tn)^{52}Mn$ reaction is small below 40 MeV. The data by Chowdhury et al. (1995) show a different shape from the other experimental data. The TENDL-2021 data agree with the experimental data up to 30 MeV. At the higher energies, the TENDL-2021 deviate in amplitude from the experimental data, though its general tendency follows the experimental data.

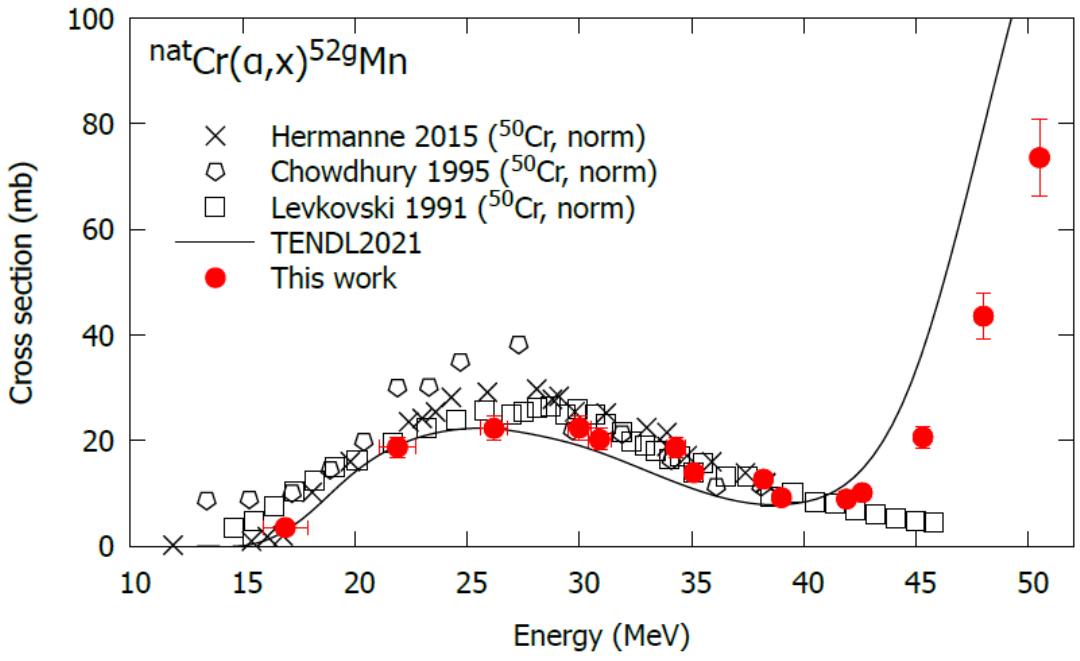

Fig. 3. Cumulative cross sections of the $^{nat}Cr(\alpha,x)^{52g}Mn$ reaction in comparison with the previous data [11-13] and the TENDL-2021 data [27]. The values, normalized for the abundance of ^{nat}Cr are shown in the figure.

3.3 The $^{nat}Cr(\alpha,x)^{54}Mn$ reaction

The γ line at 834.848 keV (I_γ = 99.9760%) from the decay of ^{54}Mn ($T_{1/2}$ = 312.20 d) was used to determine the cross sections of the $^{nat}Cr(\alpha,x)^{54}Mn$ reaction. The cross-section data were deduced from the spectra measurements performed after a cooling time of 69 hours. No decay contribution can occur for production of ^{54}Mn. Our results are compared with the previous studies [11-13] and the TENDL-2021 data library [27] in Fig. 4. The experimental cross-section data measured on $^{52,53}Cr$ target materials [12,13] were normalized to those on ^{nat}Cr for comparison. Our result shows an agreement with the previous studies and the small contribution of the $^{54}Cr(\alpha,tn)^{54}Mn$ reaction having the threshold energy of 23.6 MeV. The TENDL-2021 data reproduce a similar shape of the excitation function although they slightly underestimate the experimental data above 30 MeV.

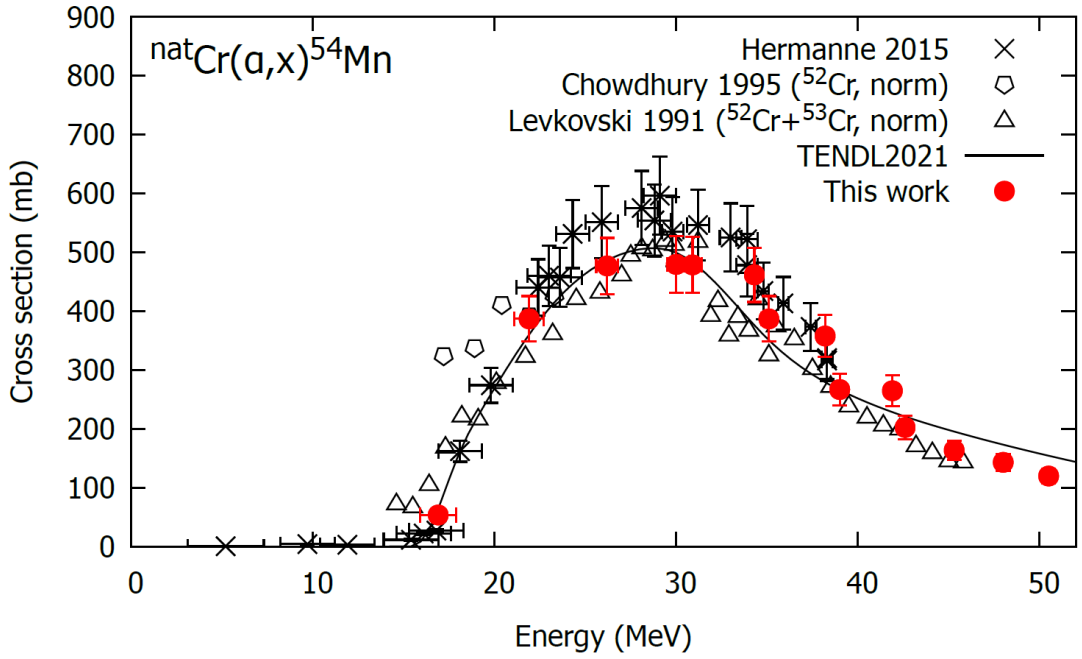

Fig. 4. Cross sections of the $^{nat}Cr(\alpha,x)^{54}Mn$ reaction in comparison with the previous data [11-13] and the TENDL-2021 data [27]. The values, normalized for the abundance of ^{nat}Cr are shown in the figure.

3.4 The $^{nat}Cr(\alpha,x)^{51}Cr$ reaction

Production of ^{51}Cr is possible in a series of reactions on all stable isotopes of chromium in the investigated energy region. The cross sections of the $^{nat}Cr(\alpha,x)^{51}Cr$ reaction were derived from the activity measurement of the 320.0824-keV γ line (I_γ = 9.910%) from the decay of ^{51}Cr ($T_{1/2}$ = 27.7025 d). The measurement series was started after a cooling time of 69 hours. The deuced cross sections are cumulative since they include the decay contribution from ^{51}Fe ($T_{1/2}$ = 305 ms) and ^{51}Mn ($T_{1/2}$ = 46.2 min). The result is shown in Fig. 5 in comparison with the previous studies [11-13] and the TENDL-2021 data [27]. The cross-section data measured on $^{50,52,53}Cr$ [12,13] were normalized to those of ^{nat}Cr for comparison. Our result is consistent with the previous studies. The contribution of the $^{54}Cr(\alpha,\alpha3n)^{51}Cr$ reaction between its threshold energy of 31.9 MeV and 45 MeV is small. The TENDL-2021 data also agree with the experimental data up to 38 MeV, however deviate in a lower amplitude from them above 38 MeV.

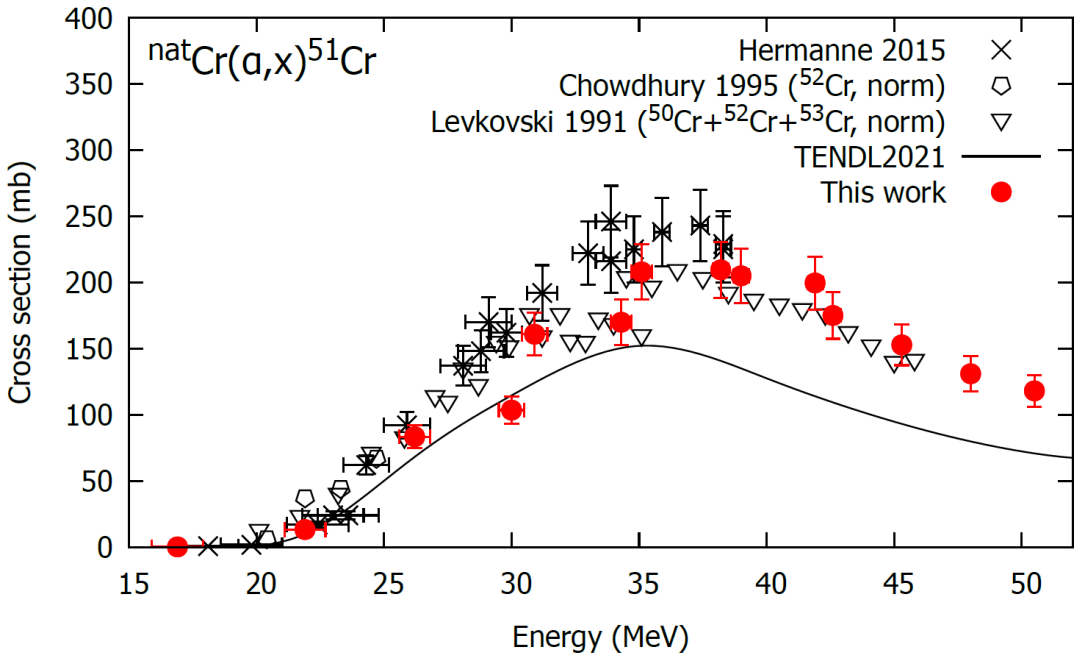

Fig. 5. Cumulative cross sections of the $^{nat}Cr(\alpha,x)^{51}Cr$ reaction in comparison with the previous data [11-13] and the TENDL-2021 data [27]. The values, normalized for the abundance of ^{nat}Cr are shown in the figure.

3.5 The $^{nat}Cr(\alpha,x)^{48}Cr$ reaction

Analysis of the γ line at 112.31 keV (I_γ = 96.0%) from the decay of ^{48}Cr ($T_{1/2}$ = 21.56 h) was performed for the γ-ray spectra recorded after a cooling time of 23 hours. The deduced cross sections of the $^{nat}Cr(\alpha,x)^{48}Cr$ reaction are compared with the previous study [13] and the TENDL-2021 data [27]. The cross section data on ^{50}Cr reported in the previous work [13] below the threshold energy of 48.3 MeV for the $^{52}Cr(\alpha,\alpha4n)^{48}Cr$ reaction were normalized to those on ^{nat}Cr. Our results are in good agreement with the previous data. The TENDL-2021 overestimates both experimental data sets. The reported cross sections include only the direct production, since the production of ^{48}Mn is a reaction that occurs above the initial bombardment energy and is energetically impossible.

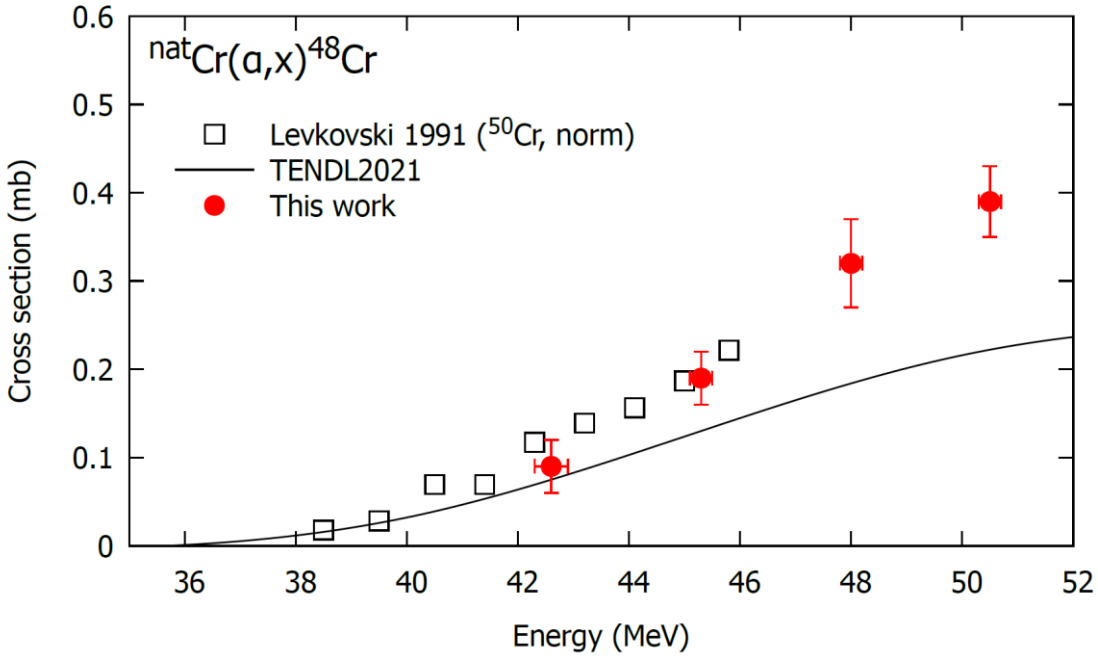

Fig. 6. Cross sections of the $^{nat}Cr(\alpha,x)^{48}Cr$ reaction in comparison with the previous data [13] and the TENDL-2021 data [27]. The values, normalized for the abundance of ^{nat}Cr are shown in the figure.

3.6 The $^{nat}Cr(\alpha,x)^{48}V$ reaction

The decay of ^{48}V ($T_{1/2}$ = 15.9735 d) is followed by emission of the γ rays at 983.525 keV (I_γ = 99.98%). To avoid the influence of that of ^{48}Cr ($T_{1/2}$ = 21.56 h), the measurement series of the γ-ray spectra was started after a cooling time of 69 hours when most of ^{48}Cr had decayed to ^{48}V. The cooling period exceeds 3 times longer than the half-life of ^{48}Cr. The contribution of ^{48}Cr was estimated using the cross sections determined in Section 3.5 and Eq. (2) in Ref. [28]. The contribution was found to be less than 3.9% and excluded from the net counts of the γ-ray spectra. Independent cross sections of the $^{nat}Cr(\alpha,x)^{48}V$ reaction were determined. The results are compared with the previous studies [11, 13] and the prediction of the model code taken from the TENDL-2021 data library [27]. The previous cross-section data measured on the ^{50}Cr targets [11, 13] were normalized to those on ^{nat}Cr by taking into account the isotope ratio listed in Table 1. Our result is consistent with the previous data. This would indicate that the contribution from the other Cr target isotopes is small at least up to 46 MeV. The TENDL-2021 data somewhat overestimate the experimental data in the whole energy range.

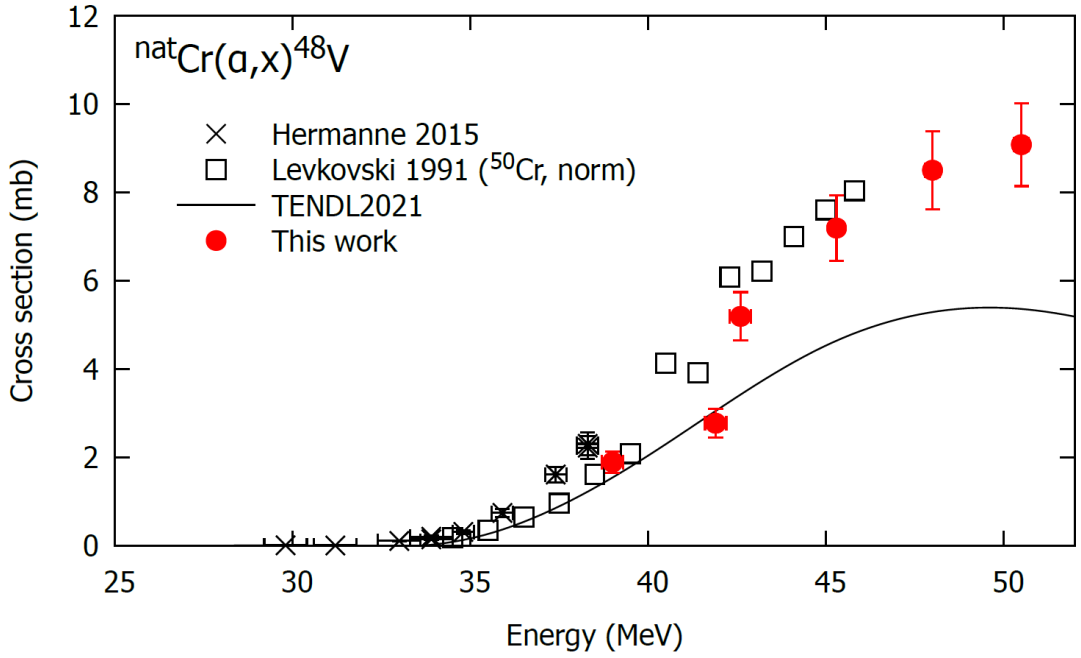

Fig. 7. Independent cross sections of the $^{nat}Cr(\alpha,x)^{48}V$ reaction compared with the previous data [11, 13] and the TENDL-2021 data [27]. The values, normalized for the abundance of ^{nat}Cr are shown in the figure.

4. Summary

We determined the activation cross sections of the α-particle-induced reactions on ^{nat}Cr. The stacked target, activation technique and high resolution γ-ray spectrometry were used. The cross sections were deduced for the ^{nat}Cr(α,x)^{52g}Fe, ^{nat}Cr(α,x)^{52g,54}Mn, ^{nat}Cr(α,x)^{48,51}Cr and ^{nat}Cr(α,x)^{48}V reactions. The newly measured data were compared with the previous experimental data and the results of the TALYS model calculation taken from the TENDL database. Our results are consistent in general with the previous experimental data.

Ethics approval and consent to participate

Not applicable

Consent for publication

Not applicable

Availability of data and materials

The datasets supporting the conclusions of this article are included within the article.

Competing interests

The authors declare that they have no competing interests.

Acknowledgements

This work was carried out at the RI Beam Factory operated by RIKEN Nishina Center and CNS, University of Tokyo Japan. This work was partly supported by JSPS KAKENHI Grant Number 17K07004. We thank Hokkaido Research Organization to conduct the elemental analysis of nickel-chromium alloy.

References

[1] Yang. Dong, Huo. Junde, Nuclear Data Sheets for A = 52, Nuclear Data Sheets, 128 (2015) 185-314.

[2] M. Lubberink, V. Tolmachev, S. Beshara, H. Lundqvist, Quantification aspects of patient studies with ^{52}Fe in positron emission tomography, Appl. Radiat. Isot., 51 (1999) 707-715.

[3] S. Beshara, J. Sorensen, M. Lubberink, V. Tolmachev, B. Langstrom, G. Antoni, B.G. Danielson, H. Lundqvist, Pharmacokinetics and red cell utilization of ^{52}Fe/^{59}Fe-labelled iron polymaltose in anaemic patients using positron emission tomography, Br. J. Haematol., 120 (2003) 853-859.

[4] P. Blauenstein, R. Pellikka, P.A. Schubiger, Reinvestigation of a physiological eluate of the ^{52}Fe/^{52m}Mn generator, Appl. Radiat. Isot., 48 (1997) 1097-1101.

[5] P. Borgies, A. Ferrant, N. Leners, J.L. Michaux, A. Bol, C. Michel, M. Cogneau, G. Sokal, Diagnosis of heterotopic bone marrow in the mediastinum using ^{52}Fe and positron emission tomography, Eur. J. Nucl. Med., 15 (1989) 761-763.

[6] S. Beshara, H. Lundqvist, J. Sundin, M. Lubberink, V. Tolmachev, S. Valind, G. Antoni, B. Langstrom, B.G. Danielson, Kinetic analysis of ^{52}Fe-labelled iron(III) hydroxide-sucrose complex following bolus administration using positron emission tomography, Br. J. Haematol., 104 (1999) 288-295.

[7] C. Calonder, P.I. Wurtenberger, R.P. Maguire, R. Pellikka, K.L. Leenders, Kinetic modeling of ^{52}Fe/^{52m}Mn-citrate at the blood-brain barrier by positron emission tomography, J. Neurochem., 73 (1999) 2047-2055.

[8] F.T. Tárkányi, A.V. Ignatyuk, A. Hermanne, R. Capote, B.V. Carlson, J.W. Engle, M.A. Kellett, T. Kibédi, G.N. Kim, F.G. Kondev, M. Hussain, O. Lebeda, A. Luca, Y. Nagai, H. Naik, A.L. Nichols, F.M. Nortier, S.V. Suryanarayana, S. Takács, M. Verpelli, Recommended nuclear data for medical radioisotope production: diagnostic positron emitters, Journal of Radioanalytical and Nuclear Chemistry, 319 (2019) 533-666.

[9] G.B. Saha, P.A. Farrer, Production of 52Fe by the ^{55}Mn(p,4n)^{52}Fe reaction for medical use, The International Journal of Applied Radiation and Isotopes, 22 (1971) 495-498.

[10] R. Capote, A.L. Nichols, F.M. Nortier, B.V. Carlson, J.W. Engle, A. Hermanne, M. Hussain, A.V. Ignatyuk, M.A. Kellett, T. Kibédi, G. Kim, F.G. Kondev, O. Lebeda, A. Luca, H. Naik, Y. Nagai, I. Spahn, S.V. Suryanarayana, F.T. Tárkányi, M. Verpelli, F.J. Hambsch, P. Schillebeeckx, W. Mondelaers, J. Heyse, S. Kopecky, P. Siegler, S. Oberstedt, IAEA coordinated research project on nuclear data for charged-particle monitor reactions and medical isotope production, EPJ Web of Conferences, 146, 08007 (2017).

[11] A. Hermanne, R. Adam Rebeles, F. Tárkányi, S. Takács, Alpha particle induced reactions on ^{nat}Cr up to 39 MeV: Experimental cross-sections, comparison with theoretical calculations and thick target yields for medically relevant ^{52g}Fe production, Nuclear Instruments and Methods in Physics Research Section B: Beam Interactions with Materials and Atoms, 356-357 (2015) 28-41.

[12] D.P. Chowdhury, S. Pal, S.K. Saha, S. Gangadharan, Determination of cross section of α-induced nuclear reaction on natural Cr and Zr by stacked foil activation for thin layer activation analysis, Nuclear Instruments and Methods in Physics Research Section B: Beam Interactions with Materials and Atoms, 103 (1995) 261-266.

[13] V. N. Levkovski, The cross-sections of activation of nuclides of middle-range mass (A=40-100) by protons and alpha particles of middle range energies (E=10-50 MeV), Inter-Vesi, Moscow, 1991.

[14] N. Otuka, E. Dupont, V. Semkova, B. Pritychenko, A.I. Blokhin, M. Aikawa, S. Babykina, M. Bossant, G. Chen, S. Dunaeva, R.A. Forrest, T. Fukahori, N. Furutachi, S. Ganesan, Z. Ge, O.O. Gritzay, M. Herman, S. Hlavač, K. Katō, B. Lalremruata, Y.O. Lee, A. Makinaga, K. Matsumoto, M. Mikhaylyukova, G. Pikulina, V.G. Pronyaev, A. Saxena, O. Schwerer, S.P. Simakov, N. Soppera, R. Suzuki, S. Takács, X. Tao, S. Taova, F. Tárkányi, V.V. Varlamov, J. Wang, S.C. Yang, V. Zerkin, Y. Zhuang, Towards a More Complete and

Accurate Experimental Nuclear Reaction Data Library (EXFOR): International Collaboration Between Nuclear Reaction Data Centres (NRDC), Nuclear Data Sheets, 120 (2014) 272-276.
[15] F. Akiha, T. Aburai, T. Nozaki, Y. Murakami, Yield of ^{52}Fe for the Reactions of 3He and α on Chromium, Radiochimica Acta, 18 (1972) 108-111.
[16] W.R. Shields, T.J. Murphy, E.J. Catanzaro, E.L. Garner, Absolute Isotopic Abundance Ratios and the Atomic Weight of a Reference Sample of Chromium, J Res Natl Bur Stand A Phys Chem, 70A (1966) 193-197.
[17] T. Watanabe, M. Fujimaki, N. Fukunishi, H. Imao, O. Kamigaito, M. Kase, M. Komiyama, N. Sakamoto, K. Suda, M. Wakasugi, K. Yamada, Beam Energy and Longitudinal Beam Profile Measurement System at RIBF, The 5th International Particle Accelerator Conference, JACoW Publishing, Dresden, Germany, 2014, pp. 3566–3568.
[18] J.F. Ziegler, M.D. Ziegler, J.P. Biersack, SRIM – The stopping and range of ions in matter (2010), Nuclear Instruments and Methods in Physics Research Section B: Beam Interactions with Materials and Atoms, 268 (2010) 1818-1823.
[19] Nuclear structure and decay data on-line library, National Nuclear Data Center, 2017.
[20] LiveChart of Nuclides, International Atomic Energy Agency, 2009.
[21] D. Abriola, M. Verpelli, J. Korean Physical Soc. 59 (2011) 1322-1324.
[22] B. Pritychenko, A. Sonzogni, Q-value Calculator, 2003.
[23] Jun Chen, Nuclear Data Sheets for A = 48, Nuclear Data Sheets, 179 (2022) 1-382.
[24] Wang Jimin, Huang Xiaolong, Nuclear Data Sheets for A = 51, Nuclear Data Sheets, 144 (2017) 1-296.
[25] Yang. Dong, Huo. Junde, Nuclear Data Sheets for A = 54, Nuclear Data Sheets, 121 (2014) 1-142.
[26] A. Hermanne, A.V. Ignatyuk, R. Capote, B.V. Carlson, J.W. Engle, M.A. Kellett, T. Kibédi, G. Kim, F.G. Kondev, M. Hussain, O. Lebeda, A. Luca, Y. Nagai, H. Naik, A.L. Nichols, F.M. Nortier, S.V. Suryanarayana, S. Takács, F.T. Tárkányi, M. Verpelli, Reference Cross Sections for Charged-particle Monitor Reactions, Nuclear Data Sheets, 148 (2018) 338-382.
[27] A.J. Koning, D. Rochman, Modern Nuclear Data Evaluation with the TALYS Code System, Nuclear Data Sheets, 113 (2012) 2841-2934.
[28] S. Takács, F. Ditrói, Z. Szűcs, M. Aikawa, H. Haba, Y. Toyoeda, G. Damdinsuren, S. Ebata, Activation cross section measurement of alpha-particle induced nuclear reactions on tantalum, Nuclear Instruments and Methods in Physics Research Section B: Beam Interactions with Materials and Atoms, 545 (2023) 165127.